doi: 10.4149/gpb_2025048

lncRNA MEG3 promotes hypoxia/reoxygenation-induced ferroptosis and cell injury in H9C2 cells through regulating the miR-22/TP53 axis

Guangyu Ma[1], Hairui Jiang[1], Meina Li[2], Caijie Li[1] and Ningning Zhang[3]

[1] *Department of Cardiology, The Second Affiliated Hospital of Qiqihar Medical University, Qiqihar, Heilongjiang Province, China*
[2] *Endocrinology Department, The First Affiliated Hospital of Qiqihar Medical University, Qiqihar, Heilongjiang Province, China*
[3] *Department of Pathophysiology, Qiqihar Medical University, Qiqihar, Heilongjiang Province, China*

Abstract. Long non-coding RNA (lncRNA) maternally expressed gene 3 (MEG3) is crucial in cerebral ischemia/reperfusion and cardiovascular cell injury. However, the effect of lncRNA MEG3 on ferroptosis due to myocardial ischemia/reperfusion is unknown. Hypoxia/reoxygenation (H/R) H9C2 cell model was constructed. qRT-PCR detected MEG3, miR-22 and tumor protein 53 (TP53) expression, and the location of MEG3 was assessed by RNA FISH. Dual luciferase assay was employed to verify whether lncRNA MEG3 targets and regulates miR-22. Cell counting kit-8 assay and EdU staining assessed cell proliferation, and flow cytometry assessed apoptosis rate. The FerroOrange fluorescent probe and Fe^{2+} assay kit were used to detect Fe^{2+} levels, and different kits to determine oxidative stress and inflammatory factors levels. Ferroptosis-related proteins levels were assessed *via* Western blot. H9C2 cell viability and proliferation were reduced, while apoptosis and pro-inflammatory factors were elevated after H/R. lncRNA MEG3 was upregulated in H/R-treated H9C2 cells, overexpression MEG3 increased Fe^{2+} and oxidative stress levels, up-regulated ferroptosis-related proteins, and knockdown MEG3 reversed the above metrics. Additionally, MEG3 regulated miR-22/TP53 axis, silencing miR-22 promoted H9C2 cell injury and ferroptosis, whereas overexpression miR-22 increased the protective impact of knockdown MEG3 on H9C2 cells. lncRNA MEG3 promotes ferroptosis caused by H/R by modulating miR-22/TP53 in H9C2 cells.

Key words: lncRNA MEG 3 — Ferroptosis — miR-22/TP53 pathway — Hypoxia/ reoxygenation — H9C2 cell

Abbreviations: ACSL4, acyl-CoA synthetase long-chain family member 4; AMI, acute myocardial infarction; CCK-8, cell counting kit-8; CK-MB, creatine kinase-MB; cTnI, cardiac troponin I; EdU, ethynyl-2'-deoxyuridine; FISH, fluorescence in situ hybridization; GPX4, glutathione peroxidase 4; H/R, hypoxia/reoxygenation; lncRNA, long non-coding RNA; MDA, malondialdehyde; MEG3, maternally expressed gene 3; MIRI, myocardial ischemia/reperfusion injury; MUT, mutant type; SLC7A11, solute carrier family 7 member 11; SOD, superoxide dismutase; TNF-α, tumor necrosis factor-alpha; IL, interleukin; UTR, untranslated region; WT, wild type.

Correspondence to: Guangyu Ma, Department of Cardiology, the Second Affiliated Hospital of Qiqihar Medical University, Zhonghua West Road, Jianhua District, Qiqihar, Heilongjiang Province, China
E-mail: Dachengzi667@126.com

© The Authors 2026. This is an **open access** article under the terms of the Creative Commons Attribution-NonCommercial 4.0 International License (https://creativecommons.org/licenses/by-nc/4.0/), which permits non-commercial use, distribution, and reproduction in any medium, provided the original work is properly cited.

Highlights:

- lncRNA MEG3 expression was elevated in H9C2 cells caused by hypoxia/reoxygenation (H/R)
- lncRNA MEG3 promoted damage and ferroptosis caused by H/R in H9C2 cells
- lncRNA MEG3 mediated miR-22/TP53 signaling
- lncRNA MEG3 promoted H9C2 cell injury and ferroptosis by mediating the miR-22/TP53 signaling pathway

Introduction

Cardiovascular disease stands as a major public health problems threatening human health worldwide, with acute myocardial infarction (AMI) becoming the most clinically dangerous subtype with the highest lethality and disability rate (Goldsborough et al. 2022; Krittanawong et al. 2023). Early reperfusion therapy can provide blood supply and nutritional support to the ischemic region, thus avoiding irreversible myocardial necrosis, making it the best option for individuals suffering from AMI (Saito et al. 2023). However, clinical practice has revealed that the reperfusion process can cause myocardial ischemia/reperfusion injury (MIRI), the pathology of which encompasses the complex physiological processes of reperfusion arrhythmia, myocardial tonus, microvascular embolism, and lethal myocardial damage (Frampton et al. 2023; Xiang et al. 2024). MIRI has now become a major influence on AMI reperfusion efficacy and patient prognosis (Liu C et al. 2023). In view of the fact that the molecular regulatory network of MIRI is still not fully understood, in-depth analysis of its pathological mechanisms and exploration of effective prevention and treatment targets have become important research directions in the cardiovascular field.

Ferroptosis, a recently uncovered type of non-apoptotic cell death, is influenced by multiple cellular metabolic pathways, like redox homeostasis regulation, amino acid metabolism, lipid peroxidation, and glycolysis (Jiang et al. 2021; Ashrafizadeh 2024). Mechanistic studies have shown that when ferroptosis occurs in cells, the abnormal accumulation of free Fe^{2+} causes a decline in glutathione peroxidase 4 (GPX4) activity, which disrupts the metabolic balance of lipid peroxides and ultimately causes an increase in reactive oxygen species (ROS) (Tang et al. 2021; Liang et al. 2022). SLC7A11 is a key protective protein that inhibits ferroptosis. Its downregulation leads to reduced cystine uptake and insufficient GSH synthesis, resulting in decreased GPX4 activity and lipid peroxidation, ultimately triggering ferroptosis (Liu H et al. 2023; Ye et al. 2023). ACSL4 activates long-chain fatty acids into acyl-CoA, providing substrates for lipid synthesis, and its high expression is considered a key marker of ferroptosis (Li et al. 2022). Research has suggested that ferroptosis is linked to AMI development, and that myocardial ischemia-reperfusion can induce ferroptosis, and ferroptosis can also exacerbate MIRI (Zhao et al. 2021; Cai et al. 2023). Therefore, interventions targeting ferroptosis may be an effective way to mitigate MIRI.

Long non-coding RNA (lncRNA), are a type of RNA that consists of over 200 nucleotides in length (Sangeeth et al. 2022). It is generally believed that lncRNAs can regulate downstream target mRNAs to affect target proteins expression and thus play a role in disease or physiological processes through various pathways, a process that may be accomplished through the competitive binding of lncRNAs to miRNAs (Yan and Bu 2021). Several lncRNAs have been found to exacerbate or alleviate MIRI symptoms in recent years (Hsieh et al. 2021; Xiao et al. 2022). Zhao et al. (2023) showed that inhibition of lncRNA maternally expressed gene 3 (MEG3) expression protects cardiovascular cells and ameliorates chronic inflammation. Importantly, Tang et al (2023) found that knockdown of MEG3 attenuated imatinib-induced cardiotoxicity and protected cardiomyocytes from damage. In addition, silencing of lncRNA MEG3 alleviated H_2O_2-caused ferroptosis in lens epithelial cells (Zhang et al. 2024). However, the impact of lncRNA MEG3 on MIRI-induced ferroptosis in cardiomyocytes and the mechanism of action are unknown.

MicroRNAs (miRNAs) are non-coding RNA molecules ranging from 10 to 22 nucleotides, which usually downregulate gene expression *via* interacting with the 3′ untranslated region (UTR) of target genes, which can cause mRNA degradation or prevent translation (Ho et al. 2022). Recent study has demonstrated that miR-22 offers protection to PC12 cells against damage caused by ischemia and subsequent reperfusion (Jiao et al. 2020). Tumor Protein 53 (TP53) gene, encodes the p53 protein, a nuclear protein with transcriptional regulatory functions and is crucial for the cellular stress responses (Voskarides and Giannopoulou 2023). Lin et al. (2023) revealed that miR-22-3p could target and downregulate TP53 and thus inhibit lung adenocarcinoma progression. Therefore, we constructed a hypoxia/reoxygenation (H/R) cell model to explore the impact of lncRNA MEG3 on ferroptosis in cardiomyocytes caused by H/R, and to investigate whether it acts by regulating miR-22/TP53 signaling. This research sought to clarify how lncRNA MEG3 functions in regulating H/R injury and to identify novel targets of action for the clinical treatment of MIRI.

Materials and Methods

Cell culture and H/R processing

Rat cardiomyoblasts (H9C2, SNL-029) were acquired from Sunncell Biotechnology (Wuhan, Hubei, China). Cells were placed in sterile culture flasks and cultured in 10% fetal bovine serum (SNS-001, Sunncell Biotechnology), 1% penicillin/streptomycin (SNA-001, Sunncell Biotechnology), 89% DMEM (SNM-002B, Sunncell Biotechnology). The temperature during incubation was set at 37°C and the incubation environment contained 95% air and 5% CO_2.

Following the methods outlined by Wang et al. (2022) and Hu et al. (2024), H9C2 cells were inoculated in 6-well plates and cultured normally for 24 h. When the cell confluence reached more than 70%, the medium was replaced with a basal medium with no sugar and no serum, and cells were transferred to an anoxic incubator with 95% N_2 and 5% CO_2, where they were maintained at 37°C for 3 h. The cells were subsequently moved to normal medium and incubated at 37°C with 5% CO_2 for 3 h to construct the H/R cell model.

MEG3 knockdown plasmid (MEG3-KD), MEG3 overexpression plasmid (MEG3-OE) and corresponding controls (MEG3-KD-NC, MEG3-OE-NC), as well as miR-22 mimics and miR-22 inhibitor were synthesized by RiboBio Co., Ltd (Guangdong, China) were synthesized. Plasmids were transfected into H9C2 cells following the instructions for Lipofectamine 3000 (L3000001, Invitrogen, Carlsbad, CA, USA). Following a 48-hour transfection period, cells were lysed sufficiently with Trizol reagent (15596018CN, Invitrogen) to extract RNA, and the efficiency of transfection was reflected by detecting MEG3 and miR-22 expression in cells.

qRT-PCR

H9C2 cells were lysed utilizing Trizol reagent to extract total RNA. Subsequently, reverse transcriptase (HY-KE8004, MedChemExpress, Monmouth Junction, NJ, USA) was applied for reverse transcription reaction to synthesize complementary DNA (cDNA). The cDNA served as a template for PCR amplification of the target gene utilizing TB Green FAST qPCR (CN830S, TAKARA, Tokyo, Japan) and by PRISM 7300 RT-PCR system (ABI, Carlsbad, CA, USA) with reference to the instructions. The target genes levels were evaluated following the $2^{-\Delta\Delta Ct}$ method, with U6 serving as an internal reference for miR-22 and MEG3, and GAPDH acts as a reference for TP53. Primer sequences were shown in Table 1.

RNA fluorescence in situ hybridization (FISH)

Referring to the method of Qin et al. (2023), the MEG3 FISH probe was designed and provided by RiboBio Co., Ltd. H9C2 cells were inoculated on coverslips and cultured until the density reached 80%, after which they were carefully rinsed with PBS. Subsequently, cell crawls were covered with 4% paraformaldehyde (P885233, Macklin, Shanghai, China) for 25 min and washed by immersion in PBS for 5 min. Cell crawls were treated with Triton X-100 (0.1%, T6328, Macklin) for 10 min to improve the permeability of the cell membrane and allow the probe to enter the cells more easily. The probe was mixed well with Hybridization Buffer (diluted at 1:50), covered the slide and incubated at 37°C overnight. Then, it was incubated with FITC-labeled streptavidin solution (A0316, Beyotime, Shanghai, China) at 37°C for 1 h and rinsed well with PBS. After the slides were dried, DAPI-Antifade Solution (P0131, Beyotime) was added dropwise, and after covering the coverslips, they were kept in darkness for 20 min, washed once. Subsequently, images were acquired using a fluorescence microscope (MF52-N, Guangzhou Micro-shot Technology Co., Ltd., Guangdong, China) in the FB-B-M channel (E_x = 470/40 nm, E_m = 530/40 nm, target RNA) and the FB-U-M channel (E_x = 375/28 nm, E_m = 460/50 nm, cell nuclei).

Nucleus extraction and isolation

Nuclei and cytoplasm were isolated by a nucleus extraction kit (ab219177, Abcam, Cambridge, MA, USA). H9C2 cells underwent treatment with 0.25% trypsin (T6325, Macklin), followed by the collection of the cell precipitate, and gently rinsed twice with PBS. Referring to the kit instructions, the cell precipitate was mixed well with 500 μl of Separation Buffer, homogenized well and centrifuged. The centrifuged precipitate contained the nucleus, and the supernatant con-

Table 1. The primer sequences utilized in this experiment

Gene	Forward primer	Reverse primer
TP53	5'-AGCACGGCCTTTGTGGTAAA-3'	5'-CCCAGCAACTACCAACCCAT-3'
GAPDH	5'-TGTAGGCTCATTTGCAGGGG-3'	5'-TCCCATTCCCCAGCTCTCTCAT-3'
MEG3	5'-GAGCTGGAATAGAGCTCGCC-3'	5'-ATTTTATGGGGCTTGCGGGA-3'
miR-22	5'-TGAGCCGCAGTAGTTCTTCAG-3'	5'-GGCAACAGTTCTTCAACTGGC-3'
U6	5'-ACCGGGGTTGCATATCATGT-3'	5'-TACAAGTGGACTGTGGCACC-3'

tained the cytoplasm, cell membrane and mitochondria. RNA was isolated from extracted nuclei and cytoplasm utilizing Trizol reagent, and the expression of MEG3 in nuclei and cytoplasm was analyzed using qRT-PCR.

Cell counting kit-8 (CCK-8) assay

H9C2 cells were seed into 96-well plates (1.5×10^4/well), and after the cells attached to the bottom of the well, they were replaced with fresh medium. Following 24 h of incubation, 10% CCK-8 reagent (HY-K0301, MedChemExpress) was introduced, shaken slightly to mix, and incubated for 2 h. OD_{450} values were assessed using microplate reader (1410101, Thermo Fisher Scientific, Waltham, MA, USA) and then calculated the cell viability.

Ethynyl-2'-deoxyuridine (EdU) staining

H9C2 cells were gently washed with PBS to remove medium residues. Added 10 μM EdU culture solution (C0075S, Beyotime), mixed thoroughly and incubated for 2 h in darkness. The cell precipitate was collected after centrifugation, gently rinsed with PBS and treated with 4% paraformaldehyde for 20 min. The cells underwent permeabilization using a 0.3% Triton X-100 solution for 15 min, and then they were incubated in the dark with the the Click reaction mixture for 25 min. The slices were blocked with AntiFade mounting medium (HY-K1047, MedChemExpress). Images were acquired under fluorescence microscopy in the FB-G-M channel (E_x = 530/40 nm, E_m = 605/55 nm, EdU-positive) and the FB-U-M channel (E_x = 375/28 nm, E_m = 460/50 nm, cell nuclei), respectively, and cell counting were performed using ImageJ1.54h software (Wavne Resband, National Institute of Mental Health, USA).

Flow cytometry

H9C2 cells were gently rinsed with PBS, and the cell precipitate was gathered by centrifugation and mixed well with Binding Buffer (500 μl). Added Annexin-V-APC (5 μl, AP107-30, Multisciences Biotech, Co., Ltd., Hangzhou, Zhejiang, China) and propidium iodide (PI, 5 μl), mixed thoroughly, and incubated for 15 min in darkness. Fluorescence intensity was assessed *via* flow cytometry (BD FACSCalibur™, BD biosciences, San Jose, CA, USA), while the evaluation of the apoptosis rate was performed using FlowJo software (v10.8, BD biosciences). The specific method was as follows: SSC-H and FSC-H were used as the primary gate to select the main cell population. For the main cell population, FL2-H (PI) and FL4-H (APC) were used as the secondary gate to analyze the proportions of cells in quadrants Q1, Q2, Q3, and Q4. The sum of the proportions of cells in quadrants Q2 and Q3 was defined as the apoptosis rate.

ELISA

Rat tumor necrosis factor-alpha (TNF-alpha, ml002859), interleukin (IL)-10 (ml037371), IL-6 (ml064292), cardiac troponin I (cTnI, ml059111) and creatine kinase-MB (CK-MB, ml059533) ELISA kits were sourced from Enzyme-linked Biotechnology (Shanghai, China). H9C2 cells supernatant were gathered by centrifugation. After adding the cell supernatant to the ELISA plate, it was left to incubate for 1.5 h. Subsequently, the appropriate antibody was introduced to each well and left to incubate for 1 h, then exposed to horseradish peroxidase-labeled Streptavidin in darkness for 20 min. Then added Substrate A and Substrate B, incubated and avoided light for 10 min, and mixed well with stop solution (50 μl), and the OD_{450} value was measured.

Cellular ultrastructure assay

After H9C2 cells were treated differently, 0.25% trypsin solution was added for digestion at 37°C for 5 min. The digestion was terminated by adding complete medium, and the cell precipitates were gathered by centrifugation. After rinsing twice with pre-cooled PBS, cells were exposed to 2.5% glutaraldehyde (G6257, Sigma-Aldrich, St. Louis, MO, USA) at 4°C overnight. After rinsing 3 times with PBS, added 1% osmium acid (O5500, Sigma-Aldrich) and fixed for 2 h away from light. Dehydration with graded ethanol (30%, 50%, 70%, 80%, 90%) for 10 min each time was followed by 100% ethanol twice. Next, the samples underwent dehydration using 100% acetone for 10 min. After dehydration, cells were embedded and placed at 60°C for 48 h of polymerization. Sections measuring 60 nm in thickness were created, stained and dried after copper mesh fished. A transmission electron microscope (HT7800, HITACHI, Tokyo, Japan) was utilized to examine the sections, and the pictures were recorded.

Measurement of Fe^{2+} levels

H9C2 cells were inoculated in 6-well cell culture plates (with built-in slides), and when the cells grew to more than 80% density, the cell slides were removed and rinsed twice. Added 1 μM FerroOrange fluorescent probe (MX4559, Maokang Biotechnology, Shanghai, China) dropwise to the surface of cell crawls, thoroughly mixed, and then allowed to incubate for half one hour in darkness. Following the reaction time, without any washing, the cells were observed under a fluorescence microscope in the FB-G-M channel (E_x = 530/40 nm, E_m = 605/55 nm), and images were captured, and the fluorescence intensity were quantified using ImageJ1.54h software.

Fe^{2+} levels were determined utilizing the Fe^{2+} Assay Kit (ab83366, Abcam). H9C2 cells were taken, trypsin digested

and resuspended in PBS. Homogenize on ice with 5 times the volume of cell suspension in iron assay buffer. The supernatant was gathered, mixed well with iron reducing agent and incubated for half an hour. Then, the iron probe was introduced, mixed well, and allowed to incubate for 1 h. Immediately after the incubation, the OD_{593} value was examined by an enzyme marker to calculate the intracellular Fe^{2+} content.

Malondialdehyde (MDA) and superoxide dismutase (SOD) levels measurement

H9C2 cell underwent a single wash with pre-cooled PBS, treated with the SOD sample preparation solution (S0101S, Beyotime), and fully lysed and centrifuged. The protein level in the supernatant was examined by a BCA protein concentration assay kit (P0012, Beyotime), and the protein level was quantified as 50 μg. Subsequently, mixed well with SOD detection buffer, treated at 37°C for 30 min, and the absorbance was assessed at 450 nm. In addition, the cell lysis supernatant was taken and the MDA level was determined following the guidelines provided by the MDA Assay kit (S0131S, Beyotime).

ROS level determination

H9C2 cells underwent two washes with PBS, followed by the addition and mixing of DCFH-DA fluorescent probe (10 μM, D6883, Sigma-Aldrich), and were then incubated in darkness for 20 min. After centrifugation, the cells were gathered, and the staining was observed *via* fluorescence microscope in the FB-B-M channel (E_x = 470/40 nm, E_m = 530/40 nm), DCFH-DA fluorescence intensity was determined *via* ImageJ1.54h software to calculate the ROS level.

Bioinformatics analysis

The potential target gene TP53 of miR-22-3p was screened by TargetScan (https://www.targetscan.org/vert_80/), miRWalk (http://129.206.7.150/) database.

Dual-luciferase reporter assay

The wild-type (WT) and mutant (MUT) dual-luciferase reporter plasmids of MEG3 3′UTR were synthesized and provided by RiboBio Co., Ltd. Lipofectamine 3000 was used to transfect WT-MEG3 and miR-22 NC, WT-MEG3 and miR-22 mimics, MUT-MEG3 and miR-22 mimics, MUT-MEG3 and miR-22 NC into H9C2 cells, respectively. Following a 48-h incubation period, the cells were gathered and the luciferase activity was assessed through the Dual-Lucy Assay Kit (RG027, Beyotime).

Western blot

RIPA lysis buffer (P0013B, Beyotime) was added to H9C2 cells to fully lyse the cells for protein extraction. After the lysis was completed, the protein level of the obtained sample was calculated through the BCA protein concentration determination kit. Next, the extracted protein supernatant was mixed well with SDS-PAGE protein loading buffer, and the proteins were separated by SDS-PAGE electrophoresis. Proteins were moved onto polyvinylidene difluoride membranes (88518, Invitrogen) and incubated with 5% bovine serum albumin for 2 h. After the washing procedure, the membrane underwent incubation overnight with the primary antibodies solute carrier family 7 member 11 (SLC7A11, PA1-16893, 1:1000, Invitrogen), Acyl-CoA synthetase long-chain family member 4 (ACSL4, ab205199, 1:1000, Abcam) or glutathione peroxidase 4 (GPX4, MA5-32827, 1:10000, Invitrogen) at 4°C. The following day, the membrane was rinsed three times and then exposed to secondary antibody (ab205718, 1:10000, Invitrogen) for 2 h. The developer (HY-K2005, MedChemExpress) was prepared according to the proportion in the instruction manual and evenly dropped on the membrane, and scanned with a gel imaging system (iBright CL1500, Invitrogen). The internal control used was GAPDH (PA1-987, 1:1000, Invitrogen). After processing the image with ImageJ software, the grayscale value of each protein band was obtained, and the relative expression level was calculated.

Statistical analysis

Every experiment was conducted a minimum of three times, and data were presented as the average ± standard deviation. The statistical evaluation was carried out using SPSS version 26.0 (IBM SPSS Statistics 26). A one-way analysis of variance (ANOVA) was utilized to conduct multiple comparisons between groups. For independent samples, if they were normally distributed, Student's *t*-test was used; otherwise, nonparametric tests were used. $p < 0.05$ represents a significant difference. Prism software (Graphpad 9.0) was used for drawing.

Results

lncRNA MEG3 expression is upregulated in H/R-treated H9C2 cells

First, we assessed MEG3 RNA expression in H9C2 cells after H/R treatment through qRT-PCR, and MEG3 expression was notably elevated after H/R (Fig. 1A). RNA FISH experiments are commonly used for localization and quantitative analysis of target RNAs in cells. We found that MEG3

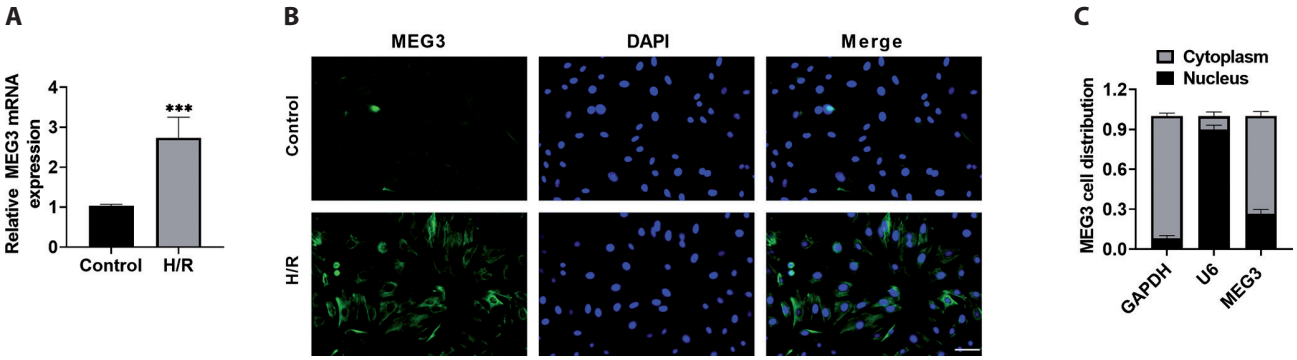


Figure 1. lncRNA MEG3 is upregulated in H/R-induced H9C2 cells. **A.** MEG3 RNA expression in H9C2 cells after H/R treatment was assessed through qRT-PCR. **B.** RNA FISH confirmed that RNA expression of MEG3 was elevated after H/R treatment and located in the cytoplasm (40×, 50 μm). **C.** MEG3 RNA expression in the nucleus and cytoplasm was detected *via* qRT-PCR, which suggested that MEG3 was expressed mainly in the cytoplasm. $n = 5$, *** $p < 0.001$ *vs.* Control.

levels were markedly elevated after H/R and located in the cytoplasm (Fig. 1B). Next, we isolated the cytoplasm and nucleus of H9C2 cells and found that MEG3 was mainly expressed in the cytoplasm, aligning with the findings of RNA FISH experiments (Fig. 1C). These findings indicated that lncRNA MEG3 was upregulated after H/R, implying that MEG3 might play a part in cell injury caused by H/R.

lncRNA MEG3 promotes H9C2 cell injury caused by H/R

To explore the influence of MEG3 on cell injury, we transfected MEG3-OE or MEG3-KD into H9C2 cells. After transfection with MEG3-OE, MEG3 expression in H9C2 cells was notably elevated, while transfection with MEG3-KD caused a marked decrease in MEG3 expression, indicating that transfection with MEG3-OE or MEG3-KD can effectively regulate the expression of MEG3 and can be used for subsequent functional experiments (Fig. 2A). CCK-8 assay findings indicated that cell viability was notably diminished after H/R, and transfection with MEG3-OE further reduced the cell viability, but transfection with MEG3-KD caused a notably increase in cell viability (Fig. 2B). Findings from EdU staining revealed that H/R treatment notably reduced EdU-positive cells number in H9C2 cells, and transfection with MEG3-OE further reduced the proliferation ability, but transfection with MEG3-KD caused a notable rise in the cell proliferation ability (Fig. 2C,D). Moreover, flow cytometry demonstrated that apoptosis rate was markedly increased after H/R, and transfection with MEG3-OE further increased the apoptosis rate, but transfection with MEG3-KD inhibited apoptosis (Fig. 2E,F). In addition, we used ELISA kits to assess biochemical markers and inflammatory factors levels in H9C2 cells. The levels of cTnI, CK-MB, IL-6, and TNF-α were markedly increased, while IL-10 level was notably decreased after H/R treatment. After transfection with MEG3-OE, cTnI, CK-MB, IL-6, and TNF-α levels were further elevated, while IL-10 level was further decreased, but transfection with MEG3-KD caused the opposite results (Fig. 2G). The above findings indicated that H/R declined H9C2 cell viability, inhibited its proliferation, and promoted apoptosis and injury, overexpression of MEG3 further promoted H9C2 cell injury, whereas knockdown of MEG3 could protect H9C2 cells.

lncRNA MEG3 promotes ferroptosis caused by H/R in H9C2 cells

Research has shown that ferroptosis is crucial in cardiomyocyte injury during H/R (Chen et al. 2023). Mitochondrial damage, elevated Fe^{2+} levels and lipid peroxidation are important hallmarks of ferroptosis (Xiao et al. 2024). Transmission electron microscopy images showed that the mitochondrial structure in H9C2 cells underwent obvious pathological changes after H/R treatment, which were characterized by distorted mitochondria, missing, fragmented and swollen mitochondrial cristae, and tiny vacuoles in the mitochondrial matrix. Overexpression of MEG3 further aggravated mitochondrial damage, while knockdown of MEG3 caused a notable decline in mitochondrial damage, with relatively intact mitochondrial cristae (Fig. 3A). Next, we used FerroOrange fluorescent probe and Fe^{2+} level detection kit to examine the impact of MEG3 on Fe^{2+} level. H/R treatment caused a marked increase in FerroOrangec fluorescence intensity and Fe^{2+} level, which was further increased by overexpression of MEG3, whereas knockdown MEG3 produced contrary results (Fig. 3B). In addition, ROS and MDA levels were notably increased, while SOD level was notably declined after H/R treatment. Transfection with MEG3-OE further elevated ROS and MDA levels and declined SOD level, but transfection with MEG3-KD weakened the effects of H/R treatment (Fig. 3C–E). Western blot results showed

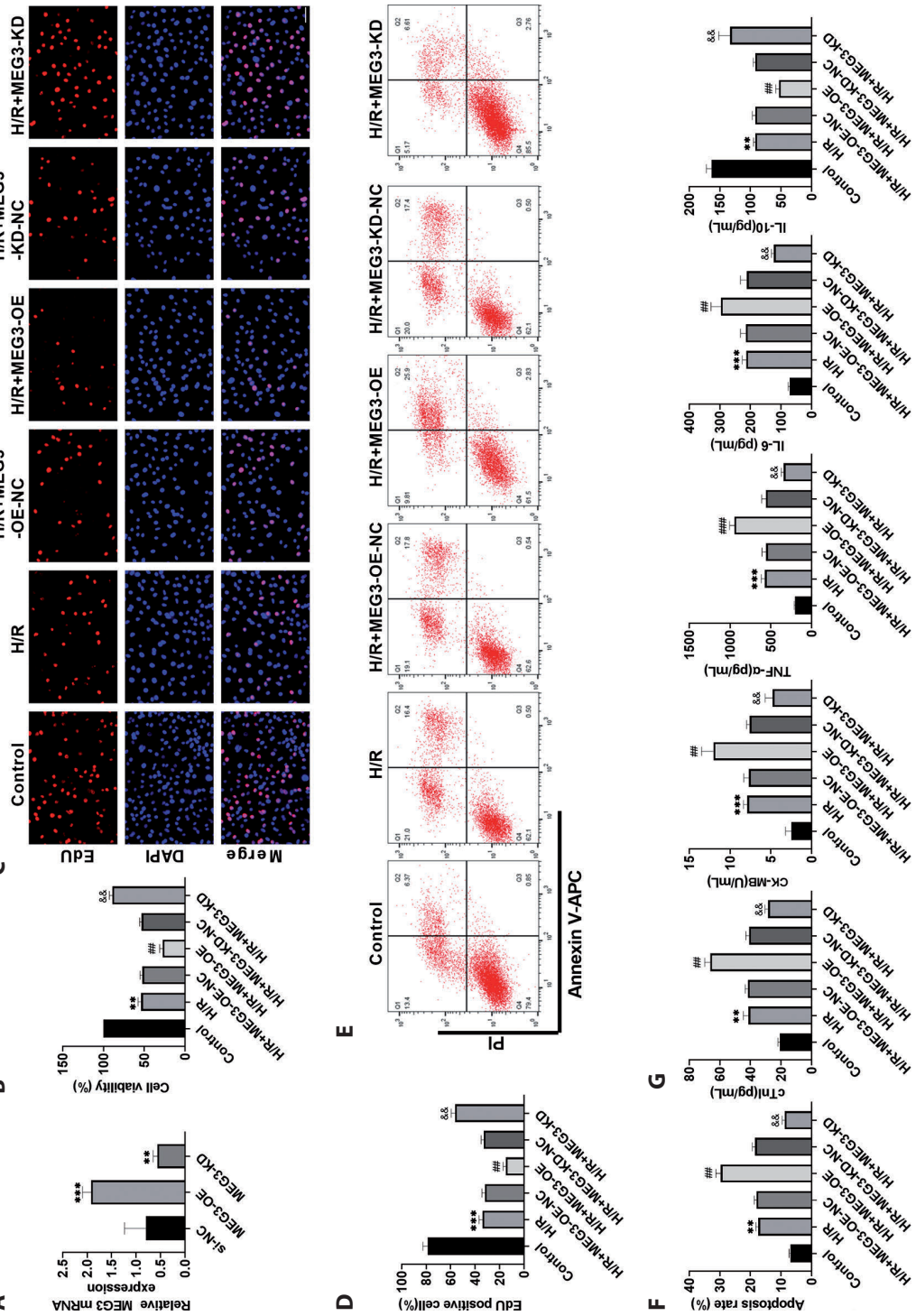


Figure 2. lncRNA MEG3 promotes H/R-treated H9C2 cell injury. **A.** MEG3-OE or MEG3-KD was transfected in H9C2 cells, and MEG3 RNA expression was assessed through qRT-PCR, confirming that transfection of MEG3-OE or MEG3-KD could effectively regulate MEG3 expression. **B.** CCK-8 assay measured that H/R treatment diminished cell viability, wand this effect was intensified by transfection with MEG3-OE, while transfection with MEG3-KD improved cell viability. **C,D.** EdU staining measured that H/R treatment diminished the EdU-positive cell rate, which was further declined by transfection with MEG3-OE, while transfection with MEG3-KD increased the EdU-positive cell rate (40×, 50 μm). **E,F.** H/R treatment resulted in increased apoptosis as measured through flow cytometry, which was further increased by transfection with MEG3-OE, whereas transfection with MEG3-KD decreased the apoptosis rate. **G.** The ELISA kits measured that H/R treatment improved cTnI, CK-MB, TNF-α, and IL-6 levels, and diminished IL-10 levels, and transfection of MEG3-OE further increased the influence of H/R treatment, while MEG3-KD diminished its effectiveness. $n = 5$, ** $p < 0.01$, *** $p < 0.001$ *vs.* Control; $^{\#\#}$ $p < 0.01$, $^{\#\#\#}$ $p < 0.001$ *vs.* H/R+MEG3-OE-NC; $^{\&\&}$ $p < 0.01$ *vs.* H/R+MEG3-KD-NC.

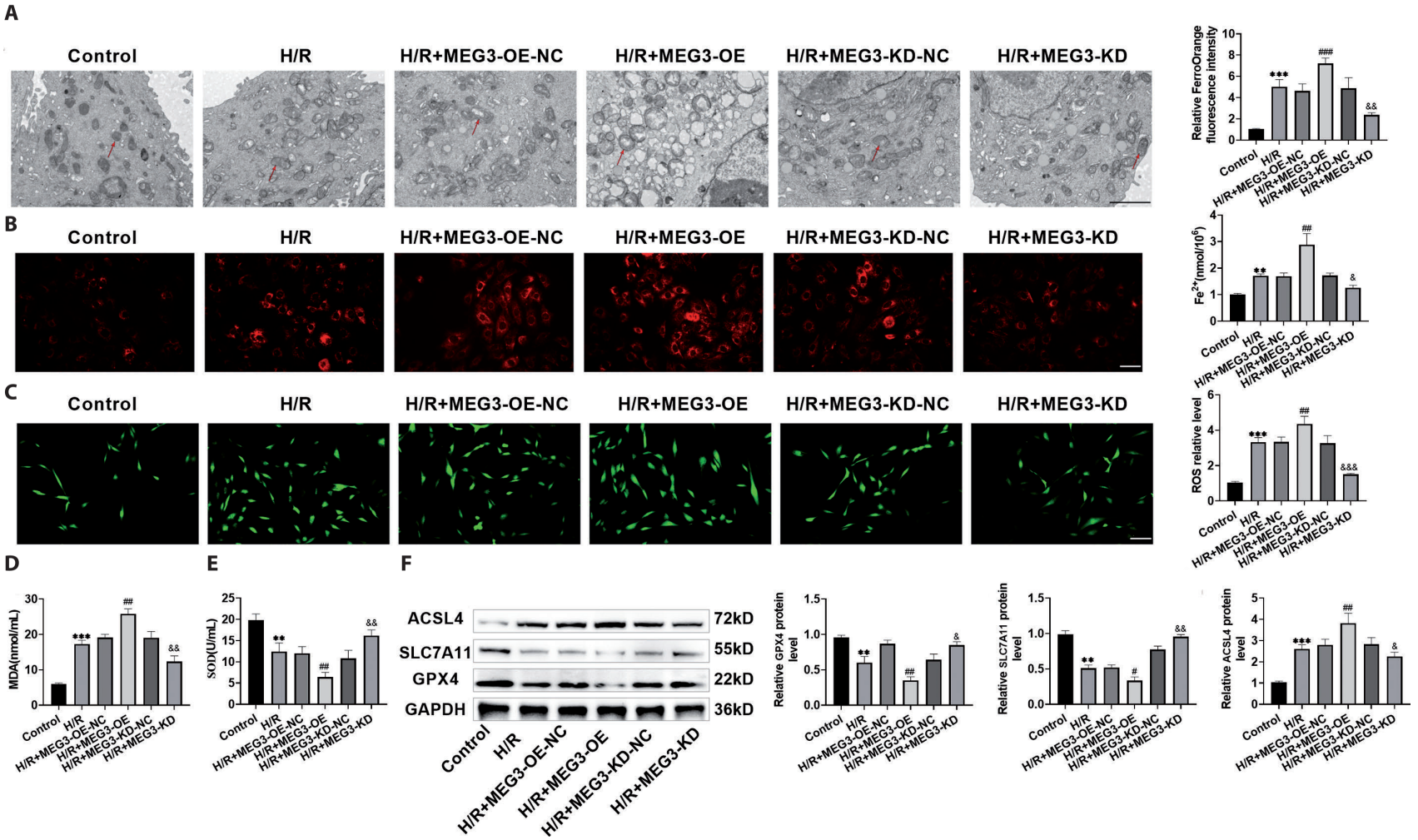


Figure 3. lncRNA MEG3 promotes H/R-induced ferroptosis in H9C2 cells. **A.** Obvious pathological changes in mitochondria after H/R treatment were observed by transmission electron microscopy, and overexpression of MEG3 further aggravated the mitochondrial damage, whereas knockdown of MEG3 alleviated the mitochondrial damage (7.0k×, 2 μm). **B.** Fe^{2+} abundance in H9C2 cells was detected using FerroOrange fluorescent probe and Fe^{2+} assay kit, which showed that Fe^{2+} abundance increased after H/R treatment, overexpression of MEG3 further increased Fe^{2+} abundance, whereas knockdown of MEG3 decreased Fe^{2+} abundance (40×, 50 μm). **C.** ROS levels were assessed using a DCFH-DA assay, ROS levels were raised by H/R treatment, overexpression of MEG3 further elevated ROS levels, and knockdown of MEG3 declined ROS levels (20×, 100 μm). The kit measured that H/R treatment raised MDA levels (**D**). and declined SOD levels (**E**), and overexpression MEG3 further increased the influence of H/R, while knockdown of MEG3 did the opposite. **F**. Western blot measured a decline in GPX4 and SLC7A11 levels and a rise in ACSL4 protein levels after H/R. Transfection of MEG3-OE further increased the impact of H/R treatment, and transfection of MEG3-KD hindered the aberrant expression of these proteins. $n = 5$, ** $p < 0.01$, *** $p < 0.001$ *vs.* Control; $^{\#}$ $p < 0.05$, $^{\#\#}$ $p < 0.01$, $^{\#\#\#}$ $p < 0.001$ *vs.* H/R+MEG3-OE-NC; $^{\&\&}$ $p < 0.01$ *vs.* H/R+MEG3-KD-NC.

that after H/R, ferroptosis inhibitory proteins SLC7A11 and GPX4 levels were markedly reduced, while ferroptosis marker protein ACSL4 level was notably increased in H9C2 cells. Transfection with MEG3-OE further enhanced the effects of H/R treatment, while transfection with MEG3-KD attenuated the abnormal expression of these proteins (Fig. 3F). The findings indicated that H/R treatment can induce ferroptosis of H9C2 cells, overexpression of MEG3 further promotes ferroptosis of H9C2 cells, and knockdown MEG3 can hinder ferroptosis caused by H/R.

lncRNA MEG3 mediates miR-22/TP53 signaling

The downstream target gene of miR-22-3p, TP53, was obtained by TargetScan and miRWalk database (Fig. 4A). Subsequently, we investigated how MEG3 influences miR-22/TP53 signaling. H/R treatment caused a notable decline in miR-22 expression level; overexpression of MEG3 further reduced miR-22 level, while knockdown MEG3 weakened the impact of H/R treatment (Fig. 4B). H/R treatment also caused a notable increase in TP53 level. Overexpression of MEG3 further increased the level of TP53, while knockdown of MEG3 weakened the impact of H/R treatment (Fig. 4C). To further detect whether MEG3 targets and regulates miR-22, we used Dual-Luciferase reporter assay to verify the targeted binding of miR-22 and MEG3. The luciferase signal in H9C2 cells was significantly declined after transfection of WT-MEG3, while transfection of MUT-MEG3 had no significant effect, further confirming that miR-22 is a downstream target gene of MEG3 (Fig. 4D). Additionally, H/R treatment caused a notable decline in miR-22 level in H9C2 cells, while knockdown MEG3 caused a rise in miR-22. Transfection of miR-22 mimics further upregulated miR-22, while miR-22 inhibitor caused a decline in miR-22 expression, indicating that MEG3 targeted negative regulation of miR-22 expression (Fig. 4E). Moreover, H/R treatment significantly elevated TP53 expression, while knockdown MEG3 caused a marked decrease in TP53 levels. Transfection of miR-22 mimics further declined TP53 expression, while transfection of miR-22 inhibitor caused upregulation of TP53 expression. These findings indicated that H/R treatment reduced miR-22 levels and increased TP53 levels, and MEG3 can regulate miR-22/TP53 signaling.

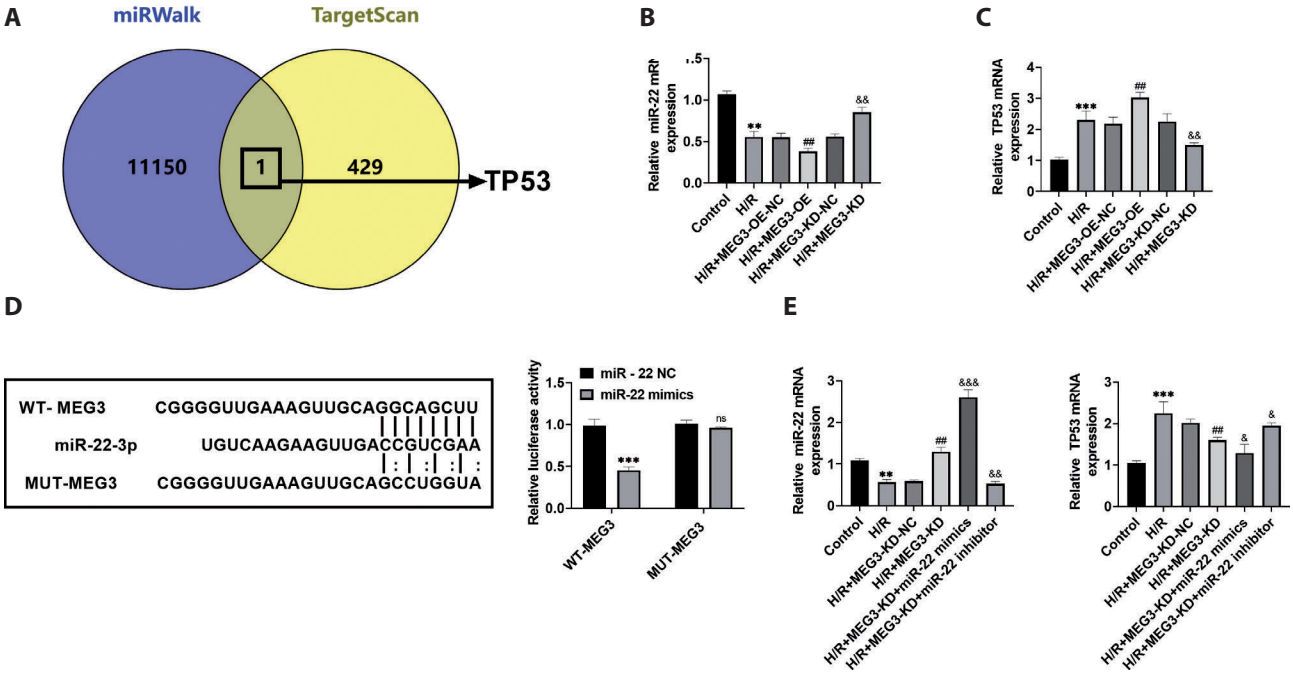


Figure 4. lncRNA MEG3 can mediate miR-22/TP53 signaling. **A.** Prediction of miR-22-3p target genes by TargetScan and miRWalk databases. H/R treatment caused a decreased miR-22 level (**B**) and raised TP53 level (**C**) in H9C2 cells as measured by qRT-PCR. Overexpression of MEG3 further enhanced the influence of H/R, while knockdown of MEG3 attenuated the impact of H/R. **D.** Dual luciferase assay confirmed miR-22 as a target of lncRNA MEG3. **E.** H/R treatment reduced miR-22 levels and increased TP53 expression as measured by qRT-PCR, whereas knockdown of MEG3 resulted in increased miR-22 levels and decreased TP53 levels, and transfection with miR-22 mimics up-regulated miR-22 level and decreased TP53, whereas the opposite was true for transfection with miR-22 inhibitor. $n = 5$, ** $p < 0.01$, *** $p < 0.001$ *vs.* Control; $^{\#}p < 0.05$, $^{\#\#}p < 0.01$, $^{\#\#\#}p < 0.001$ *vs.* H/R+MEG3-OE-NC; $^{\&\&}p < 0.01$ *vs.* H/R+MEG3-KD-NC.

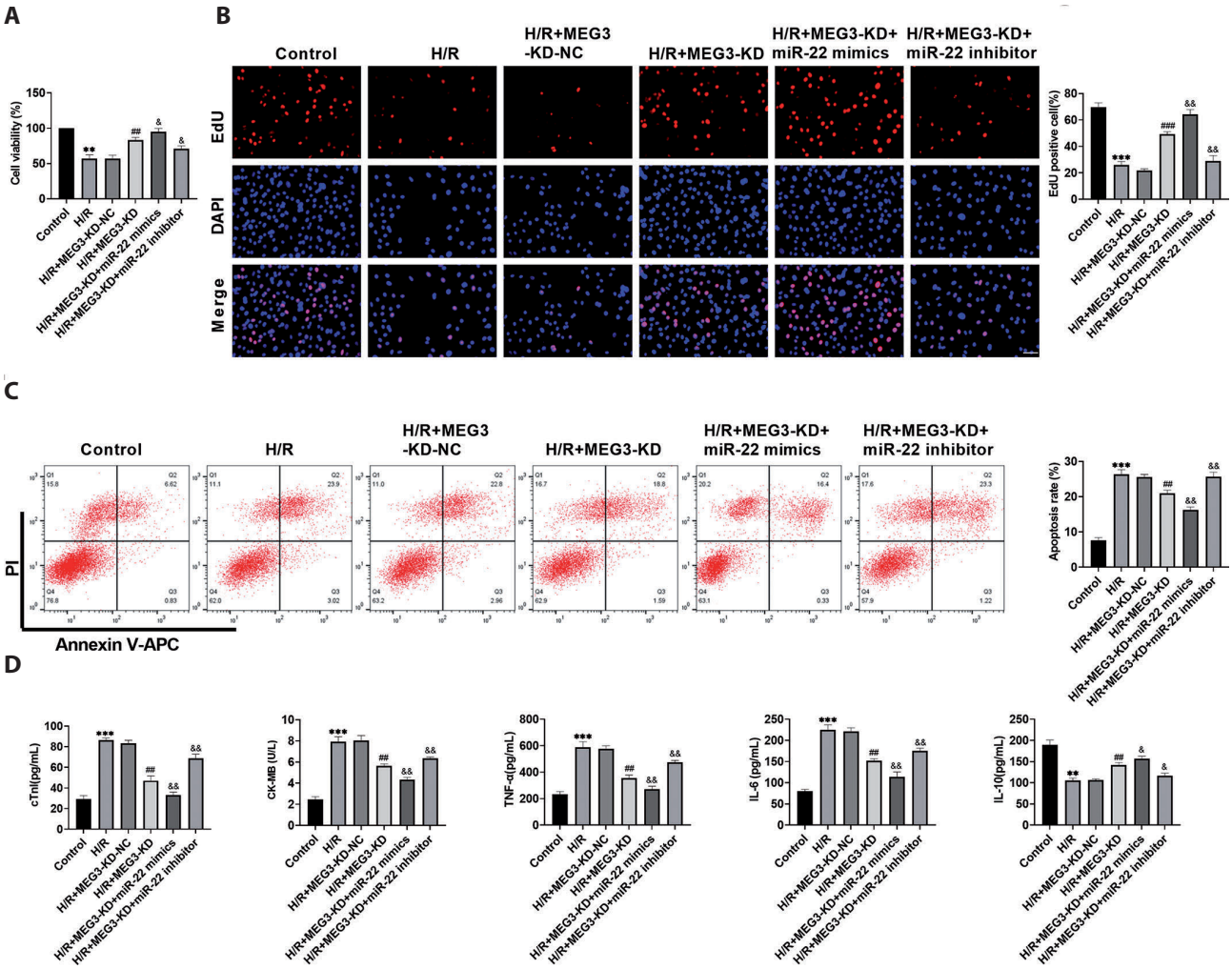


Figure 5. lncRNA MEG3 mediates miR-22/TP53 signaling to promote H9C2 cell injury induced by H/R **A.** CCK-8 assay showed that knockdown of MEG3 increased cell viability, which was further raised by transfection of miR-22 mimics, while the opposite was true for transfection of miR-22 inhibitor. **B.** EdU staining measured knockdown of MEG3 raised the rate of EdU-positive cells, which was further increased by transfection of miR-22 mimics, while miR-22 inhibitor decreased EdU-positive cells (40×, 50 μm). **C.** Knockdown of MEG3 resulted in decreased apoptosis as measured through flow cytometry, which was further decreased by transfection of miR-22 mimics, while miR-22 inhibitor raised the apoptosis rate. **D.** Knockdown of MEG3 decreased cTnI, CK-MB, IL-6 and TNF-α levels and raised IL-10 level as assessed by ELISA kits, and transfection of miR-22 mimics further raised the impact of knockdown MEG3, while miR-22 inhibitor did the opposite. $n = 5$, *** $p < 0.001$ *vs* Control; $^{\#\#}$ $p < 0.01$, $^{\#\#\#}$ $p < 0.001$ *vs* H/R+MEG3-KD-NC; $^{\&}$ $p < 0.05$, $^{\&\&}$ $p < 0.01$ *vs* H/R+MEG3-KD.

lncRNA MEG3 mediates miR-22/TP53 signaling to promote H9C2 cell injury caused by H/R

We hypothesized that MEG3 is involved in H9C2 cell injury caused by H/R through influencing miR-22/TP53 signaling. In order to assess hypothesis, we investigated the influence of overexpression or knockdown of miR-22 on H9C2 cell injury. Knockdown of MEG3 increased H9C2 cell viability, and transfection of miR-22 mimics elevated the effect of knockdown of MEG3 and further increased H9C2 cell viability, whereas transfection of miR-22 inhibitor markedly declined cell viability (Fig. 5A). Additionally, overexpression of miR-22 markedly increased EdU-positive cells, and silencing miR-22 decreased the cell proliferation ability (Fig. 5B). Not only that, overexpression miR-22 hindered H/R-caused apoptosis, and silencing miR-22 resulted in a significantly higher apoptosis rate (Fig. 5C). Notably, cTnI, CK-MB, IL-6, and TNF-α levels were notably reduced after overexpression of miR-22, and IL-10 level was markedly increased. Following silencing

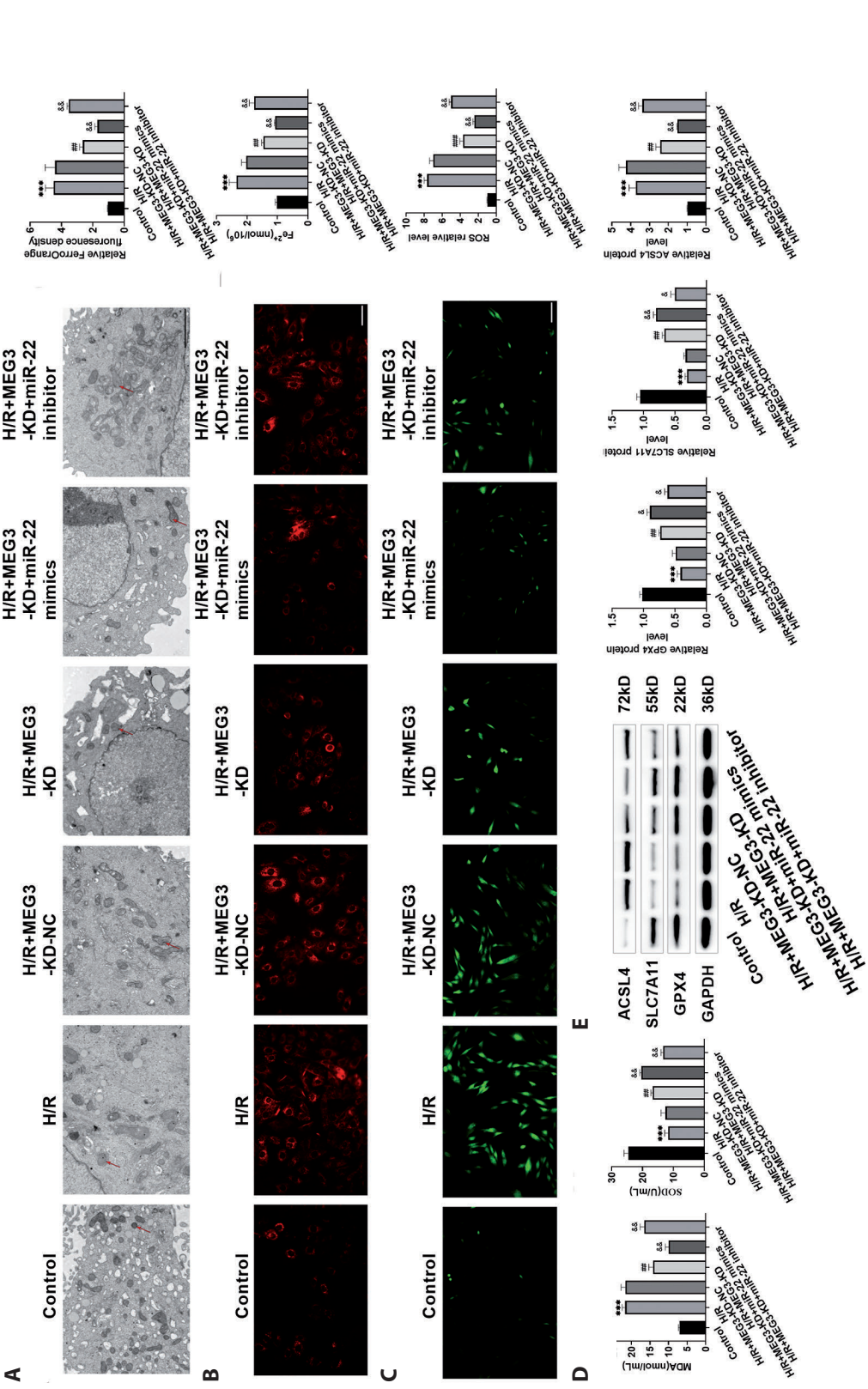


Figure 6. lncRNA MEG3 mediates miR-22/TP53 signaling pathway to promote ferroptosis in H9C2 cells induced by H/R. **A.** Knockdown of MEG3 attenuated H/R-caused mitochondrial damage as observed by transmission electron microscopy, and overexpression miR-22 further attenuated mitochondrial damage, whereas silencing of miR-22 aggravated mitochondrial damage (7.0k×, 2 μm). **B.** FerroOrange fluorescent probe and Fe^{2+} assay kit showed that knockdown of MEG3 decreased Fe^{2+} abundance in H9C2 cells, overexpression of miR-22 further declined Fe^{2+} abundance, and silencing of miR-22 raised Fe^{2+} abundance (40×, 50 μm). **C.** DCFH-DA fluorescent probe assay showed that knockdown of MEG3 decreased ROS levels, overexpression of miR-22 further decreased ROS levels, and silencing miR-22 increased ROS levels (20×, 100 μm). **D.** The kits measured that knockdown of MEG3 decreased MDA levels and increased SOD levels, and overexpression miR-22 further increased the effect of knockdown of MEG3, while silencing miR-22 did the opposite. **E.** Western blot measured that GPX4 and SLC7A11 levels were raised after knockdown of MEG3, while ACSL4 protein level was decreased. Transfection of miR-22 mimics further enhanced the impact of knockdown MEG3, and miR-22 inhibitor suppressed the aberrant expression of these proteins. $n = 5$, *** $p < 0.0001$ *vs.* Control; ## $p < 0.01$, ### $p < 0.001$ *vs.* H/R+MEG3-KD-NC; && $p < 0.01$ *vs.* H/R+MEG3-KD.

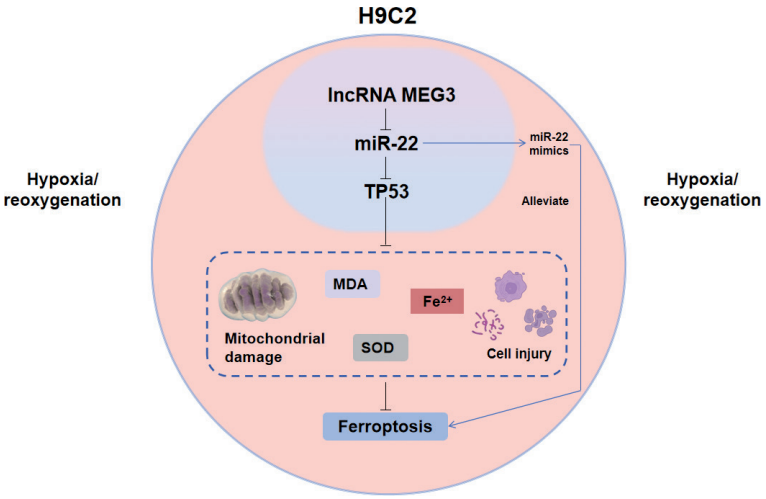


Figure 7. Mechanism of action hypoxia/reoxygenation-induced ferroptosis. lncRNA MEG3 expression was upregulated in H9C2 cells caused by H/R, and it promoted H/R-caused cell injury and ferroptosis by regulating miR-22/TP53 signaling.

miR-22, the levels of cTnI, CK-MB, TNF-α, and IL-6 were markedly increased, while IL-10 level was declined (Fig. 5D). These findings indicated that overexpression miR-22 further improved the protective impact of knockdown of MEG3 on H9C2 cells, whereas silencing of miR-22 reduced the effect of knockdown of MEG3, suggesting that MEG3 may promote cell injury caused by H/R through regulating miR-22/TP53 signaling.

lncRNA MEG3 mediates miR-22/TP53 signaling to promote H9C2 cell injury induced by H/R

Finally, we explored whether MEG3 promotes ferroptosis in H9C2 cells by modulating miR-22/TP53 signaling. Overexpression miR-22 increased the protective role of MEG3 knockdown on mitochondria, alleviated H/R-caused mitochondrial damage, and the mitochondrial cristae were more intact, while silencing of miR-22 further aggravated mitochondrial damage (Fig. 6A). Knockdown of MEG3 caused a notable decrease in Fe^{2+} levels, ROS and MDA levels and elevated SOD level, overexpression of miR-22 further improved the impact of knockdown MEG3, while silencing miR-22 was opposite (Fig. 6B–D). Notably, knockdown of MEG3 increased GPX4 and SLC7A11 levels and decreased ACSL4 level in H/R-treated H9C2 cells, whereas overexpression miR-22 further elevated the GPX4 and SLC7A11 levels and declined ACSL4 level, and silencing miR-22 attenuated the ferroptosis inhibitory effect of knockdown MEG3 on H9C2 cells inhibition (Fig. 6E). The above results indicated that overexpression miR-22 improved the impact of knockdown MEG3, while silencing of miR-22 inhibited the protective impact of knockdown MEG3 on cells, suggesting that MEG3 could promote ferroptosis in H9C2 cells through regulating miR-22/TP53 signaling.

Discussion

MIRI is a complex process with a series of pathophysiologic changes occurring after blood flow is restored to the ischemic region (Algoet et al. 2023). MIRI has been intensively studied in several countries around the world and is now generally recognized to be associated with oxidative stress, ferroptosis in cardiomyocytes, abnormalities in glycolipid metabolism, severe inflammatory responses and mitochondrial damage (Zhou et al. 2021; Tian et al. 2023). Since the specific pathogenesis of MIRI remain unclear, the therapeutic effect of targeting MIRI is not satisfactory. Therefore, in-depth investigation of its pathogenesis and exploration of potential therapeutic targets are particularly necessary and urgent. Referring to the previous research (Wang et al. 2022; Hu et al. 2024), we constructed an H/R-induced H9C2 cell model. As a structural protein specific to cardiomyocytes, cTnI binds to actin and myosin to form a complex that participates in the regulation of myocardial contraction under normal physiological conditions (Nobre Pacífico Pereira et al. 2022; Xie et al. 2023). CK-MB, a myocardial tissue-specific isoenzyme, encodes a gene that is highly selectively expressed in cardiomyocytes (Xu et al. 2020). Under physiological conditions, CK-MB participates in myocardial energy metabolism by catalyzing the reversible phosphorylation reaction between creatine and ATP, providing a critical energy buffer for myocardial contraction (Chen et al. 2021). Once cardiomyocytes are damaged due to ischemia, hypoxia, and other pathological factors, the integrity of the cell membrane is disrupted, and cTnI and CK-MB are released into the blood circulation (Alnemer 2024). Both are therefore commonly used in clinical practice to assess myocardial injury and are important indicators for the diagnosis of AMI. After H/R, the survival and proliferation of H9C2 cells were reduced, the apoptosis rate was increased, and cTnI and CK-MB levels

were also increased, so it can be judged that the H9C2 cell injury model was successfully constructed.

In recent years, lncRNA MEG3 has attracted much attention in the study of ischemic pathological mechanisms. Yao et al. (2024) demonstrated that lncRNA MEG3 could regulate the hnRNPA1/Sirt2 pathway, exacerbate mitochondrial dysfunction induced by cerebral ischemia/reperfusion, promote oxidative stress. Li et al. (2020) indicated that lncRNA MEG3 was upregulated in mouse and microglia models of cerebral ischemia/reperfusion injury, and silencing of MEG3 alleviated injury and reduced inflammatory cytokines levels and inhibited M1 macrophage polarization. Nonetheless, there is still a research gap regarding the function of lncRNA MEG3 in MIRI-induced cardiomyocyte injury. In our study, MEG3 RNA expression level was raised after H/R, and localized in the cytoplasm in H9C2 cells, implying that MEG3 might be involved in H9C2 cell injury induced by H/R. Next, we transfected MEG3 overexpression or knockdown plasmids into H9C2 cells and found that overexpression of MEG3 promoted H/R-induced impairment of H9C2 cell viability, causing declined cell viability and proliferation, elevated apoptosis, and increased cTnI, CK-MB and inflammatory factors levels. In contrast, knockdown of MEG3 attenuated H/R-induced H9C2 cell damage, suggesting that interventions targeting the lncRNA MEG3 may be a potential way to ameliorate MIRI.

Aberrant activation of ferroptosis as a new form of programmed cell death in MIRI is closely linked with cardiomyocyte injury (Gao et al. 2023; Liu C et al. 2023). Although MEG3 has been shown to affect chondrocyte ferroptosis by modulating downstream signaling pathways (Zhu et al. 2024), whether MEG3 is involved in the pathologic development of MIRI by interfering with ferroptosis remains to be explored in depth. The elucidation of this scientific question will provide a novel perspective to unravel the molecular mechanisms of MIRI and lay the theoretical foundation for the development of myocardial protection strategies targeting MEG3. Ferroptosis involves multiple mechanisms, including Fe^{2+} accumulation, lipid peroxidation, depletion of reduced glutathione, and reduced GPX4 activity (Čepelak et al. 2020). GPX4, a core enzyme in the regulation of cellular redox homeostasis, is responsible for preventing the formation of lipid peroxides, with MDA being a major product of lipid peroxidation (Ursini and Maiorino 2020). SLC7A11, a cystine/glutamate countertransporter protein, is a crucial protein in the modulation of ferroptosis, it is responsible for transporting extracellular cysteine into cells, where it is converted into cystine, and thereby promoting the synthesis of glutathione (GSH), a crucial intracellular antioxidant (Koppula et al. 2021). ACSL4 regulates the cellular lipid peroxidation response, and its upregulation causes the accumulation of lipid peroxidation products, and can exacerbate ferroptosis in cardiomyocytes and is considered a key marker and molecular target of ferroptosis (Cui et al. 2024). Previous study have demonstrated that in H9C2 cells undergoing ferroptosis, SLC7A1 expression is upregulated while ACSL4 expression is downregulated (Yang et al. 2025). In our study, H/R treatment caused ferroptosis, as evidenced by significant mitochondrial damage, elevated Fe^{2+}, ROS and MDA levels, reduced SOD levels, GPX4 and SLC7A11 expression, and elevated ACSL4 protein levels in H9C2 cells, which is in agreement with previous findings (Bai et al. 2021; Wang et al. 2022). Overexpression of MEG3 aggravated H/R treatment-induced ferroptosis, while knockdown of MEG3 reduced MDA and ROS levels, inhibited the accumulation of Fe^{2+} levels, and attenuated the aberrant expression of ferroptosis-associated proteins, suggesting that knockdown MEG3 alleviated ferroptosis induced by H/R.

Numerous researches have shown that lncRNAs can regulate various diseases or physiological processes by acting as endogenous competing RNAs, binding to miRNAs, and deregulating the post-transcriptional repression of miRNAs on mRNAs of target genes (Karagkouni et al. 2021; Zhu et al. 2023). Therefore, we hypothesized that lncRNA MEG3 may act by regulating the expression of downstream miRNAs. miR-22 is important in the pathological process of AMI and cardiac remodeling after AMI, and can effectively inhibit autophagy in cardiac cells and suppress ventricular remodeling after myocardial infarction (Gupta et al. 2016). In addition, overexpression of miR-22 inhibited tumor cell ferroptosis caused by ferroptosis inducers (Yuan et al. 2023). Notably, Su et al. (2018) found by bioinformatics analysis that lncRNA MEG3 could target to negatively regulate miR-22. miR-22 in turn can target and regulate TP53 (Lin et al. 2023), we therefore explored whether lncRNA MEG3 acts by regulating the miR-22/TP53 axis. We discovered that H/R treatment declined miR-22 levels and heightened TP53 levels, while knockdown of MEG3 resulted in increased miR-22 levels and decreased TP53 levels, suggesting that MEG3 regulates miR-22/TP53 signaling. Not only that, overexpression miR-22 improved the protective impact of knockdown MEG3 on H9C2 cells, but silencing miR-22 promoted H/R-induced injury and ferroptosis, confirming that MEG3 promotes H/R injury by regulating miR-22/TP53 signaling (Fig. 7).

Conclusion

H/R reduced H9C2 cell viability and induced its ferroptosis, and lncRNA MEG3 further exacerbated cell injury and ferroptosis process induced by H/R. Notably, we discovered a novel mechanism by which lncRNA MEG3 promotes ferroptosis by modulating miR-22/TP53 signaling, which in turn exacerbates H/R-caused H9C2 cell injury. Based on this, intervention strategies targeting lncRNA MEG3 and miR-22/TP53 signaling pathways could be a potential

therapeutic direction to combat MIRI. Despite the findings of this research, certain constraints remain, and future studies can deeply verify the mechanism of MEG3 and the specific effects of pathway regulation by constructing animal models. In conclusion, lncRNA MEG3 and miR-22/TP53 signaling provide a new research direction for MIRI treatment, warranting further exploration in future studies.

Conflict of interest. The manuscript has not been published before, and it is not being reviewed by any other journal. The authors have all approved the content of the paper. The authors affirm that they do not have any financial conflicts of interest.

Data availability statement. The data supporting the findings of this study can be obtained from the corresponding author, upon request.

Funding. Qiqihar Science and Technology Plan Joint Guidance (Grant No. LSFGG-2023083)

Authors' contributions. GM, conceived and designed the research, and analyzed data. Drafted and revised the manuscript critically for important intellectual content. Participated in the conception and design of the study. Played a key role in data interpretation and manuscript preparation. HJ, ML, CL, NZ, contributed to the acquisition, analysis, and interpretation of data. Provided substantial intellectual input during the drafting and revision of the manuscript. All authors have read and approved the final version of the manuscript.

References

Algoet M, Janssens S, Himmelreich U, Gsell W, Pusovnik M, Van den Eynde J, Oosterlinck W (2023): Myocardial ischemia-reperfusion injury and the influence of inflammation. Trends Cardiovasc. Med. **33,** 357-366 https://doi.org/10.1016/j.tcm.2022.02.005

Alnemer KA (2024): In-hospital mortality in patients with acute myocardial infarction: A literature overview. Cureus **16,** e66729 https://doi.org/10.7759/cureus.66729

Ashrafizadeh M (2024): Cell death mechanisms in human cancers: molecular pathways, therapy resistance and therapeutic perspective. JCBT **1,** 17-40 https://doi.org/10.62382/jcbt.v1i1.13

Bai YT, Xiao FJ, Wang H, Ge RL, Wang LS (2021): Hypoxia protects H9c2 cells against ferroptosis through SENP1-mediated protein DeSUMOylation. Int. J. Med. Sci. **18,** 1618-1627 https://doi.org/10.7150/ijms.50804

Cai W, Liu L, Shi X, Liu Y, Wang J, Fang X, Chen Z, Ai D, Zhu Y, Zhang X (2023): Alox15/15-HpETE aggravates myocardial ischemia-reperfusion injury by promoting cardiomyocyte ferroptosis. Circulation **147,** 1444-1460 https://doi.org/10.1161/CIRCULATIONAHA.122.060257

Čepelak I, Dodig S, Dodig D (2020): Ferroptosis: regulated cell death. Arh. Hig. Rada Toksikol. **71,** 99-109 https://doi.org/10.2478/aiht-2020-71-3366

Chen TP, Zhang NJ, Wang HJ, Hu SG, Geng X (2021): Knockdown of circROBO2 attenuates acute myocardial infarction through regulating the miR-1184/TRADD axis. Mol. Med. **27,** 21 https://doi.org/10.1186/s10020-021-00275-6

Chen W, Zhang Y, Wang Z, Tan M, Lin J, Qian X, Li H, Jiang T (2023): Dapagliflozin alleviates myocardial ischemia/reperfusion injury by reducing ferroptosis via MAPK signaling inhibition. Front. Pharmacol. **14,** 1078205 https://doi.org/10.3389/fphar.2023.1078205

Cui J, Chen Y, Yang Q, Zhao P, Yang M, Wang X, Mang G, Yan X, Wang D, Tong Z, et al (2024): Protosappanin a protects dox-induced myocardial injury and cardiac dysfunction by targeting ACSL4/FTH1 axis-dependent ferroptosis. Adv. Sci (Weinh). **11,** e2310227 https://doi.org/10.1002/advs.202310227

Frampton J, Ortengren AR, Zeitler EP (2023): Arrhythmias after acute myocardial infarction. Yale J. Biol. Med. **96,** 83-94 https://doi.org/10.59249/LSWK8578

Gao X, Hu W, Qian D, Bai X, He H, Li L, Sun S (2023): The mechanisms of ferroptosis under hypoxia. Cell Mol. Neurobiol. **43,** 3329-3341 https://doi.org/10.1007/s10571-023-01388-8

Goldsborough E, 3rd, Osuji N, Blaha MJ (2022): Assessment of cardiovascular disease risk: a 2022 update. Endocrinol. Metab. Clin. North Am. **51,** 483-509 https://doi.org/10.1016/j.ecl.2022.02.005

Gupta SK, Foinquinos A, Thum S, Remke J, Zimmer K, Bauters C, de Groote P, Boon RA, de Windt LJ, Preissl S, et al (2016): Preclinical development of a MicroRNA-based therapy for elderly patients with myocardial infarction. J. Am. Coll. Cardiol. **68,** 1557-1571 https://doi.org/10.1016/j.jacc.2016.07.739

Ho PTB, Clark IM, Le LTT (2022): MicroRNA-based diagnosis and therapy. Int. J. Mol. Sci. **23,** 7167 https://doi.org/10.3390/ijms23137167

Hsieh PF, Yu CC, Chu PM, Hsieh PL (2021): Long non-coding RNA MEG3 in cellular stemness. Int. J. Mol. Sci. **22,** 5348 https://doi.org/10.3390/ijms22105348

Hu F, Hu T, He A, Yuan Y, Wang X, Zou C, Qiao Y, Xu H, Liu L, Wang Q, et al (2024): Puerarin protects myocardium from ischaemia/reperfusion injury by inhibiting ferroptosis through downregulation of VDAC1. J. Cell Mol. Med. **28,** e70313 https://doi.org/10.1111/jcmm.70313

Jiang X, Stockwell BR, Conrad M (2021): Ferroptosis: mechanisms, biology and role in disease. Nat. Rev. Mol. Cell Biol. **22,** 266-282 https://doi.org/10.1038/s41580-020-00324-8

Jiao H, Chen R, Jiang Z, Zhang L, Wang H (2020): miR-22 protect PC12 from ischemia/reperfusion-induced injury by targeting p53 upregulated modulator of apoptosis (PUMA). Bioengineered **11,** 209-218 https://doi.org/10.1080/21655979.2020.1729321

Karagkouni D, Karavangeli A, Paraskevopoulou MD, Hatzigeorgiou AG (2021): Characterizing miRNA-lncRNA interplay. Methods Mol. Biol. **2372,** 243-262 https://doi.org/10.1007/978-1-0716-1697-0_21

Koppula P, Zhuang L, Gan B (2021): Cystine transporter SLC7A11/xCT in cancer: ferroptosis, nutrient dependency, and cancer therapy. Protein Cell **12,** 599-620

https://doi.org/10.1007/s13238-020-00789-5
Krittanawong C, Khawaja M, Tamis-Holland JE, Girotra S, Rao SV (2023): Acute myocardial infarction: etiologies and mimickers in young patients. J. Am. Heart Assoc. **12,** e029971 https://doi.org/10.1161/JAHA.123.029971
Li M, Meng Z, Yu S, Li J, Wang Y, Yang W, Wu H (2022): Baicalein ameliorates cerebral ischemia-reperfusion injury by inhibiting ferroptosis via regulating GPX4/ACSL4/ACSL3 axis. Chem. Biol. Interact. **366,** 110137 https://doi.org/10.1016/j.cbi.2022.110137
Li T, Luo Y, Zhang P, Guo S, Sun H, Yan D, Liu X, Yang B (2020): LncRNA MEG3 regulates microglial polarization through KLF4 to affect cerebral ischemia-reperfusion injury. J. Appl. Physiol. **129,** 1460-1467 https://doi.org/10.1152/japplphysiol.00433.2020
Liang D, Minikes AM, Jiang X (2022): Ferroptosis at the intersection of lipid metabolism and cellular signaling. Mol. Cell **82,** 2215-2227 https://doi.org/10.1016/j.molcel.2022.03.022
Lin R, Li GS, Gan XY, Peng JX, Feng Y, Wang LT, Zhang CY, Huang KY, Huang SH, Yang L, et al. (2023): The clinical significance and mechanism of microRNA-22-3p targeting TP53 in lung adenocarcinoma. Technol. Health Care **31,** 1691-1707 https://doi.org/10.3233/THC-220494
Liu C, Li Z, Li B, Liu W, Zhang S, Qiu K, Zhu W (2023): Relationship between ferroptosis and mitophagy in cardiac ischemia reperfusion injury: a mini-review. PeerJ. **11,** e14952 https://doi.org/10.7717/peerj.14952
Liu H, Zhang TA, Zhang WY, Huang SR, Hu Y, Sun J (2023): Rhein attenuates cerebral ischemia-reperfusion injury via inhibition of ferroptosis through NRF2/SLC7A11/GPX4 pathway. Exp. Neurol. **369,** 114541 https://doi.org/10.1016/j.expneurol.2023.114541
Liu Y, Li L, Wang Z, Zhang J, Zhou Z (2023): Myocardial ischemia-reperfusion injury: Molecular mechanisms and prevention. Microvasc. Res. **149,** 104565 https://doi.org/10.1016/j.mvr.2023.104565
Nobre Pacífico Pereira KH, Hibaru VY, Fuchs KDM, Cruz Dos Santos Correia LE, Lopes MD, Ferreira JCP, Ferreira de Souza F, Machado LHA, Chiacchio SB, Gomes Lourenço ML (2022): Use of cardiac troponin I (cTnI) levels to diagnose severe hypoxia and myocardial injury induced by perinatal asphyxia in neonatal dogs. Theriogenology **180,** 146-153 https://doi.org/10.1016/j.theriogenology.2021.12.027
Qin C, Wang T, Qian N, Liu J, Xi R, Zou Q, Liu H, Niu X (2023): Epigallocatechin gallate prevents cardiomyocytes from pyroptosis through lncRNA MEG3/TAF15/AIM2 axis in myocardial infarction. Chin. Med. **18,** 160 https://doi.org/10.1186/s13020-023-00856-z
Saito Y, Oyama K, Tsujita K, Yasuda S, Kobayashi Y (2023): Treatment strategies of acute myocardial infarction: updates on revascularization, pharmacological therapy, and beyond. J. Cardiol. **81,** 168-178 https://doi.org/10.1016/j.jjcc.2022.07.003
Sangeeth A, Malleswarapu M, Mishra A, Gutti RK (2022): Long Non-coding RNA therapeutics: recent advances and challenges. Curr. Drug Targets **23,** 1457-1464 https://doi.org/10.2174/1389450123666220919122520
Su J, Fang M, Tian B, Luo J, Jin C, Wang X, Ning Z, Li X (2018): Atorvastatin protects cardiac progenitor cells from hypoxia-induced cell growth inhibition via MEG3/miR-22/HMGB1 pathway. Acta Biochim. Biophys. Sin. (Shanghai) **50,** 1257-1265 https://doi.org/10.1093/abbs/gmy133
Tang D, Chen X, Kang R, Kroemer G (2021): Ferroptosis: molecular mechanisms and health implications. Cell Res. **31,** 107-125 https://doi.org/10.1038/s41422-020-00441-1
Tang P, Zhou J, Liu H, Mei S, Wang K, Ming H (2023): Depletion of lncRNA MEG3 ameliorates imatinib-induced injury of cardiomyocytes via regulating miR-129-5p/HMGB1 axis. Anal. Cell Pathol. (Amst.) **2023,** 1108280 https://doi.org/10.1155/2023/1108280
Tian H, Zhao X, Zhang Y, Xia Z (2023): Abnormalities of glucose and lipid metabolism in myocardial ischemia-reperfusion injury. Biomed. Pharmacother. **163,** 114827 https://doi.org/10.1016/j.biopha.2023.114827
Ursini F, Maiorino M (2020): Lipid peroxidation and ferroptosis: The role of GSH and GPx4. Free Radic. Biol Med. **152,** 175-185 https://doi.org/10.1016/j.freeradbiomed.2020.02.027
Voskarides K, Giannopoulou N (2023): The role of TP53 in adaptation and evolution. Cells **12,** 512 https://doi.org/10.3390/cells12030512
Wang Z, Yao M, Jiang L, Wang L, Yang Y, Wang Q, Qian X, Zhao Y, Qian J (2022): Dexmedetomidine attenuates myocardial ischemia/reperfusion-induced ferroptosis via AMPK/GSK-3β/Nrf2 axis. Biomed. Pharmacother. **154,** 113572 https://doi.org/10.1016/j.biopha.2022.113572
Xiang Q, Yi X, Zhu XH, Wei X, Jiang DS (2024): Regulated cell death in myocardial ischemia-reperfusion injury. Trends Endocrinol. Metab. **35,** 219-234 https://doi.org/10.1016/j.tem.2023.10.010
Xiao H, Zhang M, Wu H, Wu J, Hu X, Pei X, Li D, Zhao L, Hua Q, Meng B, et al. (2022): CIRKIL exacerbates cardiac ischemia/reperfusion injury by interacting with Ku70. Circ. Res. **130,** e3-17 https://doi.org/10.1161/CIRCRESAHA.121.318992
Xiao Z, Li S, Wu X, Chen X, Yan D, He J (2024): GATA-4 overexpressing BMSC-derived exosomes suppress H/R-induced cardiomyocyte ferroptosis. iScience **27,** 110784 https://doi.org/10.1016/j.isci.2024.110784
Xie C, Zhan Y, Wu Y, Zhang Z, Xiang Y, Wang L, Chen D (2023): Expression and clinical significance of serum sST2, BDNF, CTnI, and BUN/Cr in patients with heart failure. Altern. Ther. Health Med. **29,** 176-181
Xu C, Zhang T, Zhu B, Cao Z (2020): Diagnostic role of postmortem CK-MB in cardiac death: a systematic review and meta-analysis. Forensic. Sci. Med. Pathol. **16,** 287-294 https://doi.org/10.1007/s12024-020-00232-5
Yan H, Bu P (2021): Non-coding RNA in cancer. Essays Biochem. **65,** 625-639 https://doi.org/10.1042/EBC20200032
Yang H, Xiao G, Wang D, Xiong T, Wang J, Jing X, Xiong B, Xie J, Liu B, She Q (2025): Inhibition of HMOX1 alleviates diabetic cardiomyopathy by targeting ferroptosis. Acta Biochim. Biophys. Sin. (Shanghai) **57,** 1420-1432 https://doi.org/10.3724/abbs.2024232
Yao L, Peng P, Ding T, Yi J, Liang J (2024): m(6)A-Induced lncRNA MEG3 promotes cerebral ischemia-reperfusion injury Via

modulating oxidative stress and mitochondrial dysfunction by hnRNPA1/Sirt2 Axis. Mol. Neurobiol. **61,** 6893-6908 https://doi.org/10.1007/s12035-024-04005-x

Ye J, Lyu TJ, Li LY, Liu Y, Zhang H, Wang X, Xi X, Liu ZJ, Gao JQ (2023): Ginsenoside Re attenuates myocardial ischemia/reperfusion induced ferroptosis via miR-144-3p/SLC7A11. Phytomedicine **113,** 154681 https://doi.org/10.1016/j.phymed.2023.154681

Yuan Y, Mei Z, Qu Z, Li G, Yu S, Liu Y, Liu K, Shen Z, Pu J, Wang Y, et al (2023): Exosomes secreted from cardiomyocytes suppress the sensitivity of tumor ferroptosis in ischemic heart failure. Signal. Transduct. Target Ther. **8,** 121 https://doi.org/10.1038/s41392-023-01336-4

Zhang X, Zheng C, Zhao J, Xu X, Yao J (2024): LncRNA MEG3 regulates ferroptosis of lens epithelial cells via PTBP1/GPX4 axis to participate in age-related cataract. J. Cell Physiol. **239,** e31330 https://doi.org/10.1002/jcp.31330

Zhao H, Yang K, Zhang Y, Li H, Ji Q, Wu Z, Ma S, Wang S, Song M, Liu GH, et al. (2023): APOE-mediated suppression of the lncRNA MEG3 protects human cardiovascular cells from chronic inflammation. Protein Cell **14,** 908-913 https://doi.org/10.1093/procel/pwad017

Zhao WK, Zhou Y, Xu TT, Wu Q (2021): Ferroptosis: opportunities and challenges in myocardial ischemia-reperfusion injury. Oxid. Med. Cell Longev. **2021,** 9929687 https://doi.org/10.1155/2021/9929687

Zhou M, Yu Y, Luo X, Wang J, Lan X, Liu P, Feng Y, Jian W (2021): Myocardial ischemia-reperfusion injury: Therapeutics from a mitochondria-centric perspective. Cardiology **146,** 781-792 https://doi.org/10.1159/000518879

Zhu C, Chen B, He X, Li W, Wang S, Zhu X, Li Y, Wan P, Li X (2024): LncRNA MEG3 suppresses erastin-induced ferroptosis of chondrocytes via regulating miR-885-5p/SLC7A11 axis. Mol. Biol. Rep. **51,** 139 https://doi.org/10.1007/s11033-023-09095-9

Zhu SF, Yuan W, Du YL, Wang BL (2023): Research progress of lncRNA and miRNA in hepatic ischemia-reperfusion injury. Hepatobiliary Pancreat. Dis Int. **22,** 45-53 https://doi.org/10.1016/j.hbpd.2022.07.008

Received: June 18, 2025
Final version accepted: November 14, 2025